WILEY-VCH

Chemistry Europe
European Chemical Societies Publishing

Take Advantage and Publish Open Access

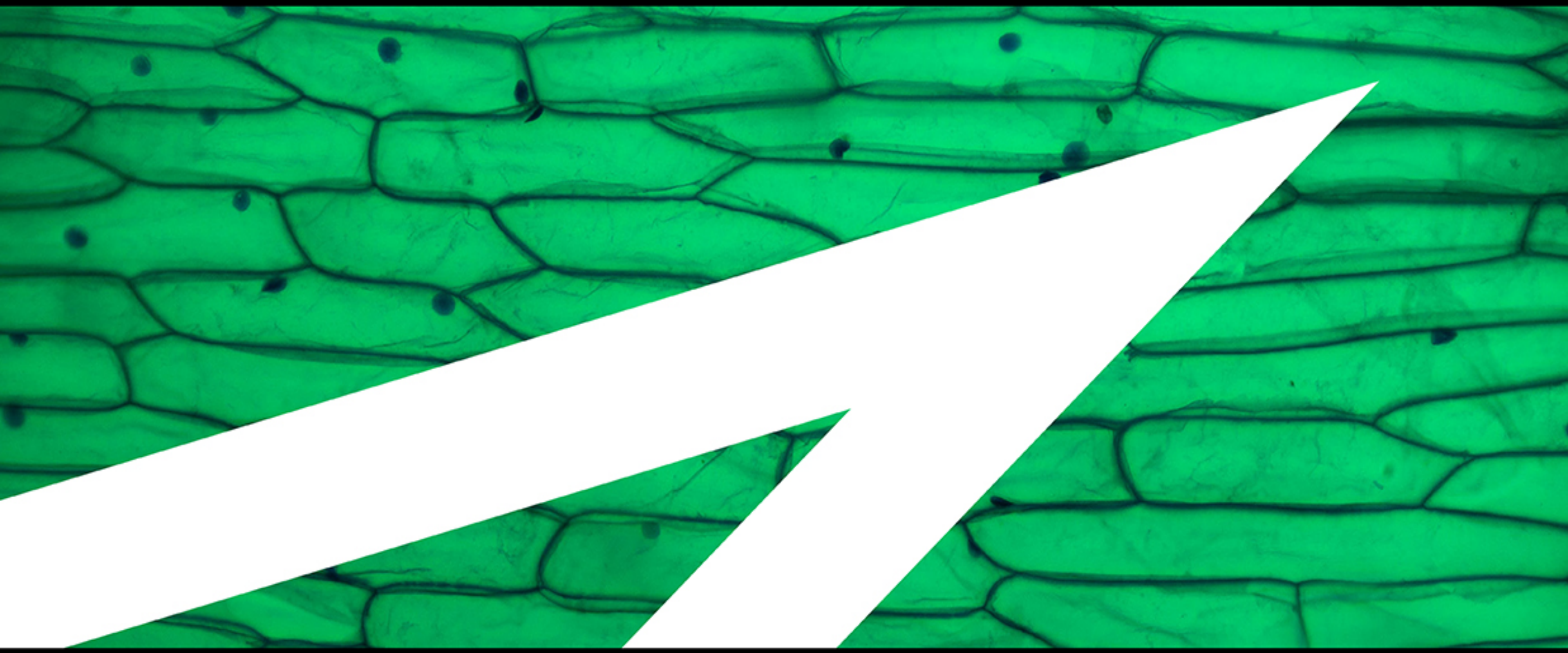

By publishing your paper open access, you'll be making it immediately freely available to anyone everywhere in the world.

That's maximum access and visibility worldwide with the same rigor of peer review you would expect from any high-quality journal.

Submit your paper today.

www.chemistry-europe.org

ChemPubSoc Europe
DOI: 10.1002/cctc.201700960
CHEMCATCHEM Full Papers

Trends of Alkane Activation on Doped Cobalt (II, III) Oxide from First Principles

Victor Fung,[a] Franklin (Feng) Tao,[b] and De-en Jiang*[a]

The surface doping of a metal oxide can tune its catalytic performance, but it remains unclear how the tuning depends on the dopant type and the surface facet. Herein we study doped Co_3O_4 (111) and (311) surface facets using first-principles density functional theory (DFT) to obtain general descriptors for oxygen reactivity (which include vacancy formation energy and hydrogen adsorption energy) and correlate them to ethane C–H activation energy as a measure of the catalytic performance. The periodic trends of the dopants are investigated for a total of 20 dopants, namely, the elements from K to Ge. We find strong linear correlations between the oxygen reactivity descriptors and the computed energy barriers. We also discover a strong surface facet sensitivity among certain dopants such that different surface orientations and sites lead to different or even the opposite dopant performance. This work provides a useful guide for dopant performance in ethane activation on the two very different Co_3O_4 surfaces.

Introduction

Metal oxides have been studied extensively for their catalytic ability in reactions such as the oxidative coupling and dehydrogenation of alkanes. These catalysts are effective in the activation of the otherwise chemically inert C–H bonds, which allows for the further conversion of the reactants. For many of these oxides, the activation occurs over the active lattice oxygen by the homolytic cleavage of the C–H bond,[1] and the resulting radicals are adsorbed onto the surface for further reaction.

As a further dimension in catalyst design, doped metal oxides have been shown to be a promising direction to tune the catalytic reactivity. Most commonly seen are substitutional dopants that replace the framework metal cation and alter the electronic structure of the neighboring atoms and thus their catalytic reactivity. Many researchers have studied the effects of doping on the reactivity of lattice oxygen theoretically. For example, McFarland and Metiu[2] concluded that lower-valence dopants increase the reactivity of the oxygen, and hence the reactivity of the surface by the Mars–van Krevelen mechanism. Meanwhile, the effects of higher-valence dopants are more complex depending on the reducibility of the oxide and the nature of the dopant.[2]

It is well known that metal oxides with different surface facets contain oxygen sites with very different activities, which must be considered to predict the catalytic performance of a metal oxide. For example, Co_3O_4 is active and stable for alkane oxidation and oxidative dehydrogenation under high temperatures.[1d,3] Depending on the synthesis and treatment method, Co_3O_4 nanoparticles of different exposed surface facet orientations can be observed with different reactivities.[3c,4] Additionally, Co_3O_4 has been doped in experimental studies in attempts to tune its reactivity and selectivity towards the desired products.[3b,5] Therefore, it is a suitable system to study and a useful starting point to understand dopant sensitivity to surface orientation.

Despite the previous work, the exact impact that different surface orientations have on dopant efficacy has not been well studied experimentally or theoretically. It is often convenient to assume that a dopant enhancing reactivity on one surface facet will do so for another on the same oxide. However, the general applicability of this assumption needs to be examined. By using Co_3O_4 as an example, we aim to study the effect of a wide range of dopants on a metal oxide systematically from first principles and to demonstrate the significance of different surface facets to determine the effect of the dopant to increase or decrease the reactivity of the metal oxide for ethane activation.

Computational Methods

The density functional theory (DFT) calculations in this work were performed by using the Vienna ab initio Simulation Package (VASP).[6] The on-site Coulomb interaction was included using the DFT+U method described by Dudarev et al.[7] in VASP using a Hubbard parameter $U = 2$ eV for the Co atom as used in previous studies.[3a,8] Theoretical studies have shown that the change of the U

---

[a] *V. Fung, Prof. Dr. D.-e. Jiang*
Department of Chemistry
University of California
Riverside, CA, 92521 (USA)
E-mail: djiang@ucr.edu

[b] *Prof. Dr. F Tao*
Department of Chemical and Petroleum Engineering and
Department of Chemistry
University of Kansas
Lawrence, KS 66045 (USA)

The ORCID identification number(s) for the author(s) of this article can be found under:
https://doi.org/10.1002/cctc.201700960.

value does not disturb the linear relationships studied in this work.[9] The Perdew–Burke–Ernzerhof (PBE)[10] form of the generalized-gradient approximation (GGA) was used for electron exchange and correlation. All calculations were performed with spin polarization. The projector-augmented wave method was used to describe the electron–core interaction.[6a, 11] The kinetic energy cutoff was set at 450 eV for the planewave basis set. For the studied surface slabs, a 3×3×1 sampling of the Brillouin zone using a Monkhorst–Pack scheme was employed.[12] A vacuum layer of 15 Å was created for the surface slabs. The top two layers of the slabs were allowed to relax in the calculations. The vacancy formation energy (E_{vac}) was calculated with Equation (1)

$$E_{vac} = E_{vacancy\,surface} + 1/2\, E_{O_2} - E_{perfect\,surface} \tag{1}$$

in which $E_{vacancy\,surface}$ is the energy of the surface slab with the oxygen atom removed, $E_{perfect\,surface}$ is the energy of the vacancy-free surface, and E_{O_2} is the energy of an isolated O_2 molecule. The hydrogen adsorption energy (E_{Hads}) is calculated with Equation (2)

$$E_{Hads} = E_{surface+H} - (E_{perfect\,surface} + E_H) \tag{2}$$

in which $E_{surface+H}$ is the energy of the surface with a H atom adsorbed on the O atom and E_H is the energy of an isolated H atom. The energies of E_{O_2} and E_H were computed by placing the adsorbate in a cubic cell with a 10 Å wide vacuum in each direction. Transition states (TS) were found by the dimer method implemented in the VASP-VTST package by Henkelman and Jónsson[13] using a force convergence criterion of 0.05 eV Å^{-1}.

Results and Discussion

Two facets of Co_3O_4 and localization of dopant effects

We examined both a flat surface, (111), and a rough surface, (311), of Co_3O_4, and their surface models are shown in Figure 1. The dopant replaces the Co atom at the location labeled "Site". We found no significant local structural change on either facet after doping, probably because of the comparatively low dopant concentration used. The oxygen coordination number of the metal is three on the (111) site and five on the (311) site. The doping is expected to change the activities of these oxygen atoms. A simple descriptor of their activity is the oxygen-vacancy formation energy, E_{vac}.

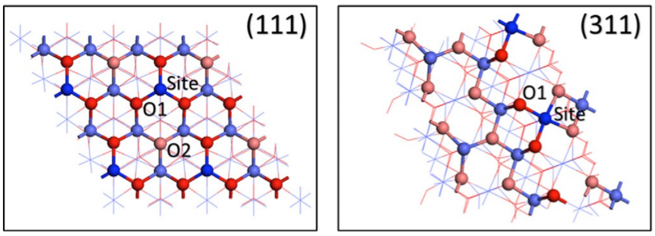

Figure 1. Surface models for the (111) surface (left) and the (311) surface (right) of Co_3O_4, in which the upper layer atoms are shown as circles and the sublayer atoms as lines. The blue atoms denote Co and the red atoms denote O. The dark blue atoms are the exposed Co sites and one is replaced by a dopant at the location labeled "Site". The nearest-neighbor O atom studied is labeled O1 and the second-nearest-neighbor is labeled O2.

We obtained E_{vac} on the first neighbors O1 and second neighbors O2 on the (111) surface and found that changes in O1 E_{vac} can be significant among dopants, whereas the O2 E_{vac} energies remain largely unchanged (Figure 2). In other words, the effect of doping is rather local and limited to the nearest-neighbor O atoms, and the impact on the O atoms beyond the first coordination shell is very weak. This is largely consistent with an earlier theoretical study on the CeO_2 surface.[14] Consequently, we focus our study on the nearest-neighbor O atom (O1).

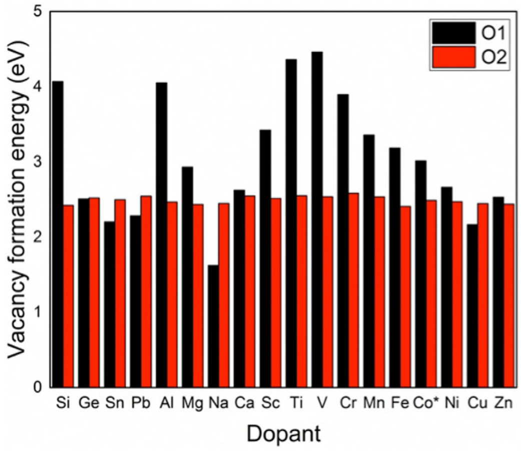

Figure 2. Vacancy formation energies of O atoms on the doped Co_3O_4 (111) surface. Co* denotes the undoped surface. O1 represents the O first neighbors and O2 represents the O second neighbors (see Figure 1).

Charge transfer between dopant and oxygen

From the perspective of the electronic structure, we can track the partial transfer of electrons from the metal to the neighboring O atoms using Bader charges. The dopant Bader charge versus the oxygen Bader charge for both the (111) and (311) facets is plotted in Figure 3. We can see the strong linear corre-

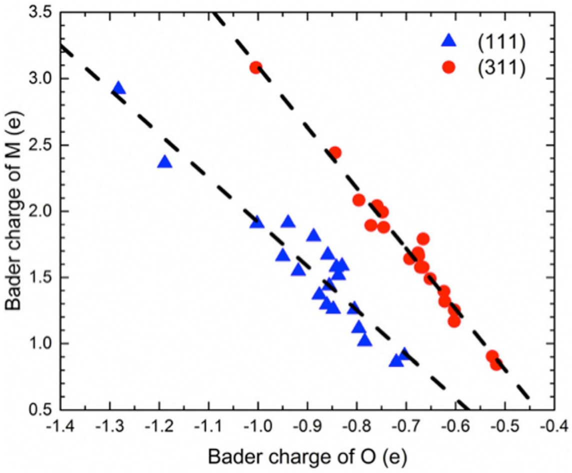

Figure 3. Bader charge of the dopant M versus the Bader charge of the nearest-neighbor O. The blue triangles and red circles denote points from the (111) and (311) surfaces of Co_3O_4, respectively. Black dashed lines represent linear best fit lines for the two surfaces.

lation between the electron loss of the lattice metal or dopant and the electron gain of the lattice oxygen, regardless of the identity of the metal dopant used. Furthermore, it suggests that the change in the lattice oxygen charge is caused directly by the change of the identity of the dopant used and not a result of geometric reconstruction or the formation of a new coordination after doping, which would result in large deviations from the linear correlation. We can also distinguish the correlation of charge transfer as two distinct lines that correspond to the (111) and (311) surfaces (Figure 3). This can be explained by the difference in the oxygen coordination of the dopant site on the (111) and (311) surfaces, namely, three and five, respectively. Consequently, the electron transfer for the dopant on the (311) surface is further dispersed among two extra O atoms, which would shift the line to the right and generate a larger slope.

Descriptors and trends of oxygen reactivity for the doped surfaces

A number of descriptors have been proposed as possible descriptors of oxygen reactivity in metal oxides, which include the energetic quantities E_{Hads}[9,15] and E_{vac}[3a,15a,16] and electronic ones such as Bader charge[8a,17] and work function.[9] E_{Hads} and E_{vac} show strong linear correlations with a low mean absolute error (MAE) of 0.16 eV and $R=0.93$ (Figure 4). This is consistent with the general observation that the correlation between E_{Hads} and E_{vac} is independent of the change of the identity of the metal in the metal oxide, or its surface orientation, and can be applied generally, because both are energetic descriptors to predict the reactivity of the oxygen site. Here we will base our analysis of oxygen reactivity on both E_{Hads} and E_{vac} as descriptors.

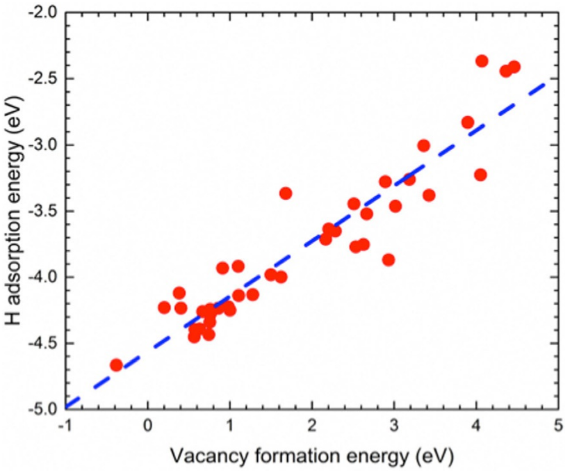

Figure 4. Correlation between H adsorption energy and vacancy formation energy for the oxygen sites closest to the dopant sites on the Co_3O_4 surfaces. The blue dashed line represents the linear best fit line.

We examine the dopant periodic trends on the oxygen reactivity descriptors and C–H activation energy for a series of elements in the same period. These trends are displayed in Figure 5 for both E_{Hads} and E_{vac}. Overall, it appears that the oxygen reactivity is the highest (i.e., most negative E_{Hads} or smallest E_{vac}) for group 1 (with K as the dopant) for both surfaces and decreases sequentially to a peak at V for (111) or Cr for (311) before it increases in activity again until Zn. Oxygen reactivity decreases again at Ga, though the dopant effect is mixed for Ge for different surfaces. Importantly, the peaks in oxygen reactivity differ in location between the two surfaces, which indicates that the surfaces on which the dopants reside in may have an important role on its reactivity. This phenomenon is further explored below. A volcano trend can be observed in Figure 5 with peaks at Ti/V for (111) and Cr for (311). From left to right, the oxidation state of the elements increases, which corresponds to stronger M–O bonds, to lead to more positive E_{Hads} and E_{vac}. As the dopant occupies the tetrahedral +2 site on (111) and the octahedral +3 site on (311), the peak of the volcano for (311) is shifted to the right. To the right of the volcano, E_{Hads} and E_{vac} become more negative as the oxidation states decrease to Zn and increase again for Ga and Ge.

C–H activation on doped surfaces

Generally for alkane activation on Co_3O_4 and other oxides, the first step of the reaction involves C–H activation, regardless of the subsequent pathways through oxidative dehydrogenation or complete combustion. Although both homolytic and heter-

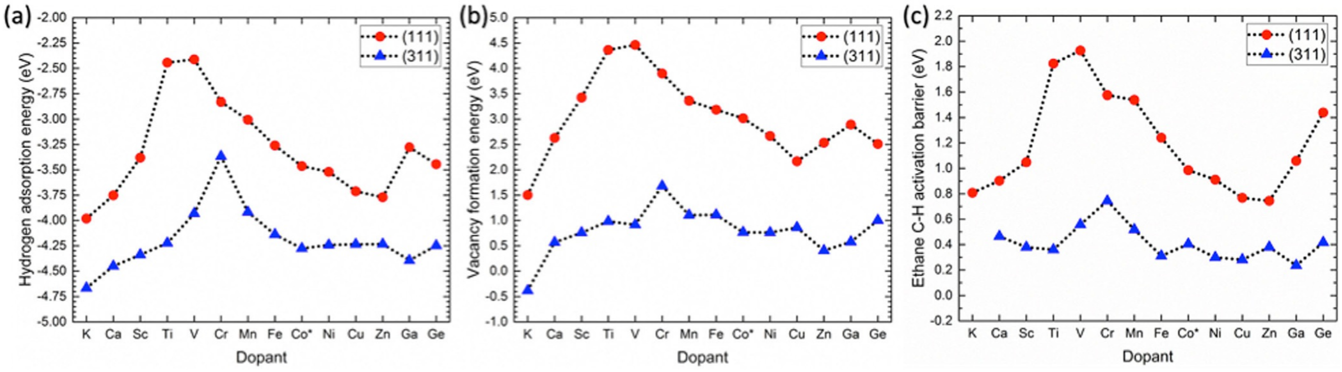

Figure 5. Periodic trends of oxygen reactivity on the M-doped Co_3O_4 surfaces: a) H adsorption energy; b) vacancy formation energy; c) C–H activation energy. Co* denotes the undoped surface.

olytic bond cleavage mechanisms are possible, studies have found that the homolytic pathway is often the pathway with the lowest barriers on Co_3O_4,[3c,8a] which involves H abstraction and cleavage of the C–H bond over a lattice O atom. It is this pathway that allows the easy prediction of C–H barriers through Brønsted–Evans–Polanyi (BEP) relations. Furthermore, it has been shown that the activation barriers of alkanes and alcohols of different chemical compositions can be related linearly to one another simply as a function of the C–H bond strength;[15b] therefore, it is possible to extrapolate results from a single alkane to the entire class of compounds. Herein we focus our efforts on homolytic C–H activation using ethane as our probe molecule.

Representative transition–states (TS) geometries for the homolytic C–H activation over the undoped (111) surface and the (311) surface are shown in Figure 6. The TS takes the form of an ethane molecule with an elongated C–H bond with the H atom situated in between the C atom and the lattice O atom. Both exhibit similar geometries and differ mainly in the TS O*–H and C–H distances and their corresponding E_a. The bond lengths of the transition states are plotted against E_{Hads} in Figure 7. The trends are apparent as E_{Hads} becomes more negative (i.e., stronger) and the lattice O atom becomes more reactive, the TS O*–H distance increases and the TS C–H distance decreases. This observation is consistent with the BEP relationship as the TS of H abstraction is an overlap between the potential energy surfaces of C–H bond dissolution and O–H bond formation. In our case (Figure 6), the strength of the C–H bond is roughly constant, whereas the strength of the O–H bond varies with the different dopants. If the oxygen reactivity is high, the TS is early, so the C–H bond is short and the O–H bond is long; if the oxygen reactivity is low, the TS is late, so the C–H bond is long and the O–H bond is short. This phenomenon, in the context of C–H bond activation on metal oxides, has been brought up in a previous theoretical study[15c] and can now be verified in terms of a general linear scaling relationship (Figure 7).

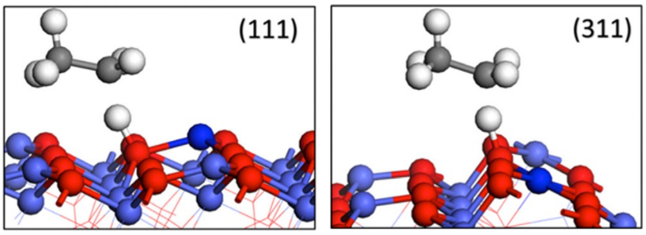

Figure 6. TS geometries of ethane C–H activation by H abstraction for the (111) surface and the (311) surface.

Correlation between C–H activation and oxygen descriptors

Many recent theoretical studies[15a,b,18] have demonstrated the validity of oxygen descriptors such as vacancy formation and H adsorption to predict C–H activation barriers. The trend of the ethane C–H activation energy (E_a) across the periodic table for both doped Co_3O_4 (111) and (311) facets is shown in Figure 5c. The overall trends of E_{Hads}, E_{vac}, and E_a across the different dopants are similar. Indeed, E_a has very strong linear correlations with both E_{Hads} and E_{vac} with a mean absolute error (MAE) of 0.15 and 0.11 eV, respectively (Figure 8). These small MAE values suggest that it is promising to use these oxygen reactivity descriptors as a method to screen dopants before expensive transition-state search calculations. One can refer to the BEP relationship to understand this correlation from the perspective of E_{Hads}.

Surface facet sensitivity of different dopants

The C–H activation energy difference between the (111) and (311) surfaces for the different dopants is shown in (Figure 9). Overall, both undoped and doped (311) surfaces are more reactive than the corresponding (111) surfaces for the C–H activation of ethane. More specifically, Ti, V, and Si show the highest sensitivity to the facets with $\Delta E_a \approx 1.3$–1.4 eV. If we use the undoped Co_3O_4 surfaces as a reference, K, Cr, Mn, Fe, Ga, and Fe also display a significantly high sensitivity to the facets. Fig-

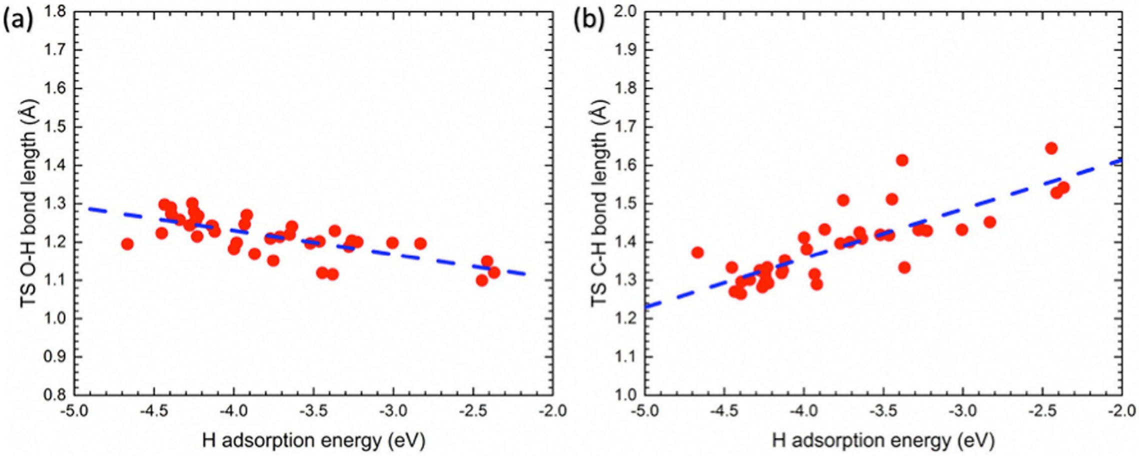

Figure 7. Correlation of the TS geometry of ethane C–H activation with H adsorption energy on doped Co_3O_4 surfaces: a) O–H bond length; b) C–H bond length. The blue dashed lines represent the linear best fit for the points.

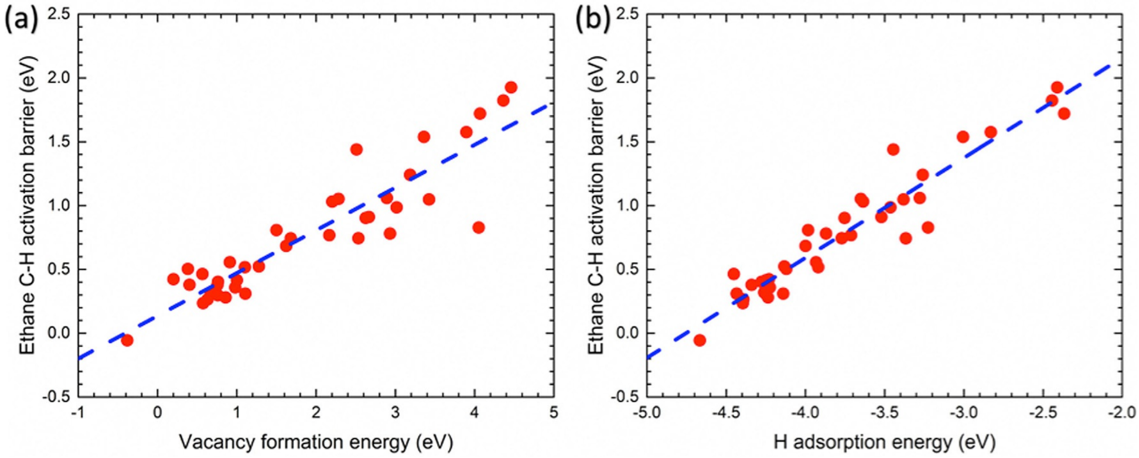

Figure 8. Correlation of the ethane C–H activation energy with: a) vacancy formation energy; b) H adsorption energy. The blue dashed lines represent the linear best fit for the points.

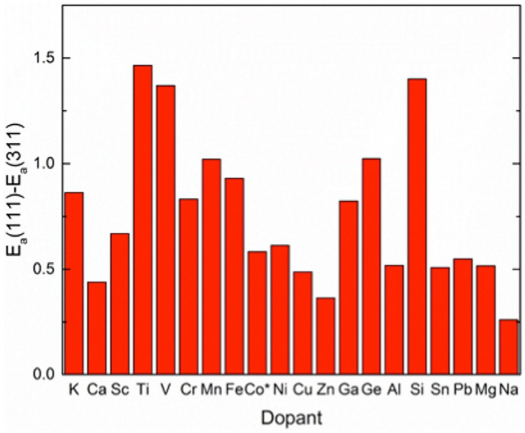

Figure 9. Difference in ethane C–H activation energy between the (111) and (311) facets for the different dopants.

ure 5c shows that Ga-doped Co_3O_4 (311) surface has the highest reactivity for the ethane C–H activation, with an activation energy close to 0.20 eV.

Implications of the present results

In this work, we have compared two surfaces, a low-index (111) surface with exposed tetrahedral Co^{2+} and a high-index (311) surface with exposed octahedral Co^{3+}, which is sufficient to demonstrate large differences in dopant effects qualitatively between the two. It is very probable that this phenomenon will extend to metal oxides in general beyond Co_3O_4. Further systematic studies on other metal oxides can be useful to develop a sufficiently comprehensive understanding to link the geometric and electronic structure of the dopant site to the oxygen reactivity through the sampling and study of a larger number of surface facets and corresponding substitution sites. The importance of surface orientation to determine dopant performance has significant implications towards the prediction of the catalytic properties of doped oxides. As different experimental synthesis techniques can lead invariably to nanoparticles with various exposed surfaces, the role of a dopant can be complicated by the surface facet sensitivity.

Here we considered a fixed dopant concentration. We expect that the scaling relation between the computed barriers and the descriptors would remain for different dopant concentrations, but testing this hypothesis would require substantially more calculations. Further studies are warranted.

Conclusions

The effects of the doping of Co_3O_4 on oxygen reactivity and C–H activation barriers were investigated for a range of dopants on two different surfaces, (111) and (311). We found the dopant effects to be limited to the nearest-neighbor O atoms with no significant changes to oxygen reactivity at or beyond the second coordination shell. The periodic trends of doping on oxygen reactivity were examined by correlating oxygen-vacancy formation, H adsorption energy on oxygen, and homolytic C–H activation energy of ethane. The oxygen reactivity descriptors (vacancy formation and H adsorption energies) were linked to the C–H activation energies and the transition-state geometry. The surface orientation can have a significant impact on dopant efficacy. This work demonstrates that oxygen activity descriptors can be used to predict dopant performance on transition metal oxide surfaces and that doping and the surface orientation can be combined to tune the reactivity of the transition metal oxide.

Acknowledgements

This work was supported by the Chemical Sciences, Geosciences and Biosciences Division, Office of Basic Energy Sciences, Office of Science, U.S. Department of Energy under Grant No. DE-SC0014561. This research used resources of the National Energy Research Scientific Computing Center, a DOE Office of Science User Facility supported by the Office of Science of the U.S. Department of Energy under Contract No. DE-AC02-05CH11231.

Conflict of interest

The authors declare no conflict of interest.

Keywords: alkanes · C–H activation · cobalt oxide · doping · surface chemistry

[1] a) J. H. Lunsford, *Angew. Chem. Int. Ed. Engl.* **1995**, *34*, 970–980; *Angew. Chem.* **1995**, *107*, 1059–1070; b) H. Schwarz, *Angew. Chem. Int. Ed.* **2011**, *50*, 10096–10115; *Angew. Chem.* **2011**, *123*, 10276–10297; c) S. Feyel, J. Döbler, D. Schröder, J. Sauer, H. Schwarz, *Angew. Chem. Int. Ed.* **2006**, *45*, 4681–4685; *Angew. Chem.* **2006**, *118*, 4797–4801; d) W. Hu, J. Lan, Y. Guo, X.-M. Cao, P. Hu, *ACS Catal.* **2016**, *6*, 5508–5519.

[2] E. W. McFarland, H. Metiu, *Chem. Rev.* **2013**, *113*, 4391–4427.

[3] a) J. Liu, S. Zhang, Y. Zhou, V. Fung, L. Nguyen, D.-e. Jiang, W. Shen, J. Fan, F. F. Tao, *ACS Catal.* **2016**, *6*, 4218–4228; b) F. F. Tao, J. J. Shan, L. Nguyen, Z. Wang, S. Zhang, L. Zhang, Z. Wu, W. Huang, S. Zeng, P. Hu, *Nat. Commun.* **2015**, *6*, 7798; c) E. C. Tyo, C. Yin, M. Di Vece, Q. Qian, G. Kwon, S. Lee, B. Lee, J. E. DeBartolo, S. Seifert, R. E. Winans, R. Si, B. Ricks, S. Goergen, M. Rutter, B. Zugic, M. Flytzani-Stephanopoulos, Z. W. Wang, R. E. Palmer, M. Neurock, S. Vajda, *ACS Catal.* **2012**, *2*, 2409–2423; d) H.-F. Wang, D. Wang, X. Liu, Y.-L. Guo, G.-Z. Lu, P. Hu, *ACS Catal.* **2016**, *6*, 5393–5398.

[4] a) L. Hu, Q. Peng, Y. Li, *J. Am. Chem. Soc.* **2008**, *130*, 16136–16137; b) Z. Chen, C. X. Kronawitter, B. E. Koel, *Phys. Chem. Chem. Phys.* **2015**, *17*, 29387–29393; c) H. Sun, H. M. Ang, M. O. Tadé, S. Wang, *J. Mater. Chem. A* **2013**, *1*, 14427–14442; d) Y. N. Sun, J. W. Liu, J. J. Song, S. S. Huang, N. T. Yang, J. Zhang, Y. H. Sun, Y. Zhu, *ChemCatChem* **2016**, *8*, 540–545; e) V. Fung, F. Tao, D.-E. Jiang, *J. Phys. Chem. Lett.* **2017**, *8*, 2206–221.

[5] a) M. Zhou, L. Cai, M. Bajdich, M. García-Melchor, H. Li, J. He, J. Wilcox, W. Wu, A. Vojvodic, X. Zheng, *ACS Catal.* **2015**, *5*, 4485–4491; b) M. Hamdani, R. N. Singh, P. Chartier, *Int. J. Electrochem. Sci.* **2010**, *5*, 556; c) C. Ohnishi, K. Asano, S. Iwamoto, K. Chikama, M. Inoue, *Catal. Today* **2007**, *120*, 145–150; d) K. Asano, C. Ohnishi, S. Iwamoto, Y. Shioya, M. Inoue, *Appl. Catal. B* **2008**, *78*, 242–249; e) Z. Shang, M. Sun, S. Chang, X. Che, X. Cao, L. Wang, Y. Guo, W. Zhan, Y. Guo, G. Lu, *Appl. Catal. B* **2017**, *209*, 33–44; f) Z. Zhu, G. Lu, Z. Zhang, Y. Guo, Y. Guo, Y. Wang, *ACS Catal.* **2013**, *3*, 1154–1164; g) Y. Lou, L. Wang, Z. Zhao, Y. Zhang, Z. Zhang, G. Lu, Y. Guo, Y. Guo, *Appl. Catal. B* **2014**, *146*, 43–49; h) Y. Lou, X.-M. Cao, J. Lan, L. Wang, Q. Dai, Y. Guo, J. Ma, Z. Zhao, Y. Guo, P. Hu, *Chem. Commun.* **2014**, *50*, 6835–6838.

[6] a) G. Kresse, J. Furthmuller, *Comput. Mater. Sci.* **1996**, *6*, 15–50; b) G. Kresse, J. Furthmuller, *Phys. Rev. B* **1996**, *54*, 11169–11186.

[7] S. Dudarev, G. Botton, S. Savrasov, C. Humphreys, A. Sutton, *Phys. Rev. B* **1998**, *57*, 1505.

[8] a) V. Fung, F. F. Tao, D.-E. Jiang, *Catal. Sci. Technol.* **2016**, *6*, 6861–6869; b) D. E. Jiang, S. Dai, *Phys. Chem. Chem. Phys.* **2011**, *13*, 978–984.

[9] G. Kumar, S. L. J. Lau, M. D. Krcha, M. J. Janik, *ACS Catal.* **2016**, *6*, 1812–1821.

[10] J. P. Perdew, K. Burke, M. Ernzerhof, *Phys. Rev. Lett.* **1996**, *77*, 3865.

[11] P. E. Blöchl, *Phys. Rev. B* **1994**, *50*, 17953–17979.

[12] H. J. Monkhorst, J. D. Pack, *Phys. Rev. B* **1976**, *13*, 5188.

[13] G. Henkelman, H. Jónsson, *J. Chem. Phys.* **1999**, *111*, 7010.

[14] Z. Hu, H. Metiu, *J. Phys. Chem. C* **2011**, *115*, 17898–17909.

[15] a) M. D. Krcha, A. D. Mayernick, M. J. Janik, *J. Catal.* **2012**, *293*, 103–115; b) A. A. Latimer, A. R. Kulkarni, H. Aljama, J. H. Montoya, J. S. Yoo, C. Tsai, F. Abild-Pedersen, F. Studt, J. K. Nørskov, *Nat. Mater.* **2017**, *16*, 225–229; c) P. Deshlahra, E. Iglesia, *J. Phys. Chem. C* **2016**, *120*, 16741–16760; d) P. Deshlahra, E. Iglesia, *ACS Catal.* **2016**, *6*, 5386–5392; e) R. A. V. Santen, M. Neurock, S. G. Shetty, *Chem. Rev.* **2010**, *110*, 2005–2048.

[16] a) M. Harth, R. Mitdank, D. Habel, O. Görke, M. Tovar, H. Winter, H. Schubert, *Int. J. Mater. Res.* **2013**, *104*, 657–665; b) B. Li, H. Metiu, *J. Phys. Chem. C* **2010**, *114*, 12234–12244; c) A. R. Derk, B. Li, S. Sharma, G. M. Moore, E. W. McFarland, H. Metiu, *Catal. Lett.* **2013**, *143*, 406–410.

[17] G.-L. Dai, Z.-P. Liu, W.-N. Wang, J. Lu, K.-N. Fan, *J. Phys. Chem. C* **2008**, *112*, 3719–3725.

[18] M. D. Krcha, M. J. Janik, *Catal. Sci. Technol.* **2014**, *4*, 3278.

Manuscript received: June 10, 2017
Revised manuscript received: July 27, 2017
Accepted manuscript online: July 28, 2017
Version of record online: November 15, 2017